

Processing of metals and semiconductors by a femtosecond laser-based microfabrication system

M. Meunier^a, B. Fisette^a, A. Houle^a, A. V. Kabashin^a, S. V. Broude^b, P. Miller^b

^aLaser Processing Laboratory, Department of Engineering Physics, Ecole Polytechnique de Montréal, Case Postale 6079, succ. Centre-ville, Montréal (Québec), H3C 3A7, Canada

^bResonetics Inc., 4 Bud Way, Nashua, NH 03063, USA

ABSTRACT

A microfabrication system with the use of a femtosecond laser was designed for 3D processing of industrially important materials. The system includes a 120 fs, 1 kHz laser; beam delivery and focusing system, systems for automated 3D target motion and real-time imaging of the sample placed in a vacuum chamber. The first tests of the system on the processing of stainless steel and silicon are presented. We established thresholds and regimes of ablation for both materials. It was found that at relatively low laser fluences $I < 3\text{-}5 \text{ J/cm}^2$ the regime of “gentle” ablation takes place, which is characterized by exceptional quality of the ablated surface, but slow ablation rate ($< 25 \text{ nm/pulse}$). This regime is especially efficient for the patterning of markers on steel or silicon surfaces. The “fast” ablation regime at $I > 10 \text{ J/cm}^2$ provides much higher ablation rate of 30-100 nm/pulse, giving an opportunity of fast high-quality processing of materials. This regime is well suited for drilling of through holes and fast cutting of materials. However, it was found that fast ablation regime imposes additional requirements on the quality of delivery and focusing of the laser beam because of the presence of parasitic ablation around the main spot on the tail of the radiation intensity distribution. As industrial machining examples, we demonstrate heat-affected-zone free drilling of through holes in a 50 μm thick stainless steel foil and cutting of a 50 μm thick Si wafer with a net cutting speed of 8 $\mu\text{m/sec}$.

Keywords: femtosecond laser ablation, laser microfabrication, stainless steel, silicon.

1. INTRODUCTION

The interaction of the femtosecond radiation with different materials is now intensively studied in many laboratories around the world. It is accepted that the femtosecond pulses give two major advantages to micromachining compared to nanosecond and longer pulses¹: (i) the reduction of the pulse energy which is necessary to induce ablation for fixed laser wavelength and focussing conditions and (ii) a significant reduction or complete removal of heat-affected zone (HAZ) and, as consequence, the improvement of the contour sharpness for the laser-processed structures. The second advantage is a direct consequence of the pulse being much shorter than the heat diffusion time. Primarily, these advantages were mentioned in experiments with PMMA². Owing to the rapid progress in femtosecond laser design, numerous materials like superconductors³, metals⁴, semiconductors⁵, ceramics⁶, dielectrics⁷, technical⁸ and biological composite materials⁹ were investigated soon afterwards. However, many aspects of the femtosecond ablation remain unclear, while the regimes of the processing of some industrially important materials are not yet optimized.

In this paper, we designed an automated femtosecond laser-based microfabrication system to process different materials. In addition, we present preliminary tests on the processing of stainless steel and silicon.

2. SYSTEM DESCRIPTION

The main task in the development of this system was to create a tool most versatile for applied materials research. As such, the system has to be somewhere between an experimental setup with its flexibility and accessibility, and a full-fledged industrial micromachining tool with its high reliability, ease of operation and throughput. Collaboration between Ecole Polytechnique de Montreal and Resonetics Inc. started with development of a set of specifications listed in Table 1.

Table 1
Specifications of the femtosecond laser processing system

| | |
|--|--|
| <u>Laser</u> | Spectra-Physics (Mountain View, CA) Hurricane ultra-compact tunable Ti-Sapphire regenerative amplifier system |
| | Output wavelength 760 nm – 820 nm (Factory settable) |
| | Output pulse energy 1.00 mJ @1 kHz |
| | Pulse width < 120 fs |
| | Output beam diameter 7 mm (at 1/e ²) |
| <u>Optics layout for two separate working areas</u> | |
| (a) Adjustable well-focussed spot delivered to a small vacuum chamber with motion control | |
| (b) Expanded laser beam (7 – 21 mm dia) delivered to a large free volume within the system for future utilization (e.g., large vacuum chamber) | |
| <u>Beam Delivery System</u> | |
| | Spot size on sample 5 – 15 µm for (a) |
| | Energy control Attenuation from OD0 to OD4 (coarse and fine) |
| <u>Motion System</u> | |
| | Sample XY stage travel (⊥ to beam): 100 mm x 100 mm |
| | Focussing lens Z stage travel (to beam) 5 mm |
| | Stage repeatability ± 2 µm bi-directional |
| | Stage stepping resolution ± 0.1µm |
| | Maximum XY velocity 50 mm/s |
| | Orthogonality of motions ± 10 arcsec |
| | Sample rotary stage Manual |
| <u>Vision System</u> | |
| | Camera On-line, on-axis viewing of process area |
| | Monitor B/W |
| <u>User Interface</u> | |
| Simple operation control menu, and Advanced process control menu CNC controller for synchronizing laser firing and x-y table movement | |
| <u>Laser Safety Compliance</u> | |
| 21 CFR, Class 4 laser system, | |
| <u>Environmental Conditions</u> | |
| | Operating temperature range 15 – 30 °C |
| | Temperature stability for best performance ± 2 °C |
| | Humidity range 0 – 95 % (non-condensing) |

From optical engineering side, the main task was to design beam-forming and -delivering system capable of producing the required spot sizes on the sample while preserving the shortness of femtosecond pulses. The following considerations have to be taken into account: (i) Gaussian laser beam propagation, (ii) Geometrical aberrations, (iii) Chromatic aberration correction, (iv) Group velocity dispersion (GVD) and third order dispersion (TOD), (v) Radial chromatic front distortion, (vi) Self phase modulation, (vii) Whole beam self-focussing. Careful balance of the above allowed for construction of a relatively simple optical system, consisting of a Galilean multi-configuration expander and a single objective for all spot sizes. All mirrors in the system are broadband “ultra-fast” mirrors optimized for 800 nm region and fabricated by CVI (Albuquerque, NM). In order to monitor and optimize femtosecond laser performance in this micro-machining system, an autocorrelator is employed (SSA, Positive Light, Los Gatos, CA). It was found impractical to monitor the focussed beam inside or close to the sample in the vacuum chamber. Instead, a dummy set of optical flats was fabricated, using the same glasses and element thicknesses as the focussing optics. For monitoring, the beam is directed into the autocorrelator through this dummy optics.

Mechanically, the system is based on an open H-frame concept to permit the highest amount of flexibility for the user while preserving its structural rigidity. The H-frame is mounted on top of vibration isolation feet to provide for dampening of external disturbances. As indicated in Fig.1, the H-frame has three major shelves (i) The top shelf with the laser and the safety shutter, (ii) The middle shelf with all the beam forming optics, attenuators, process shutter, pulse characterization tools, the focussing optics and the vision system, (iii) The bottom shelf with the vacuum sample chamber, and the motion stages.

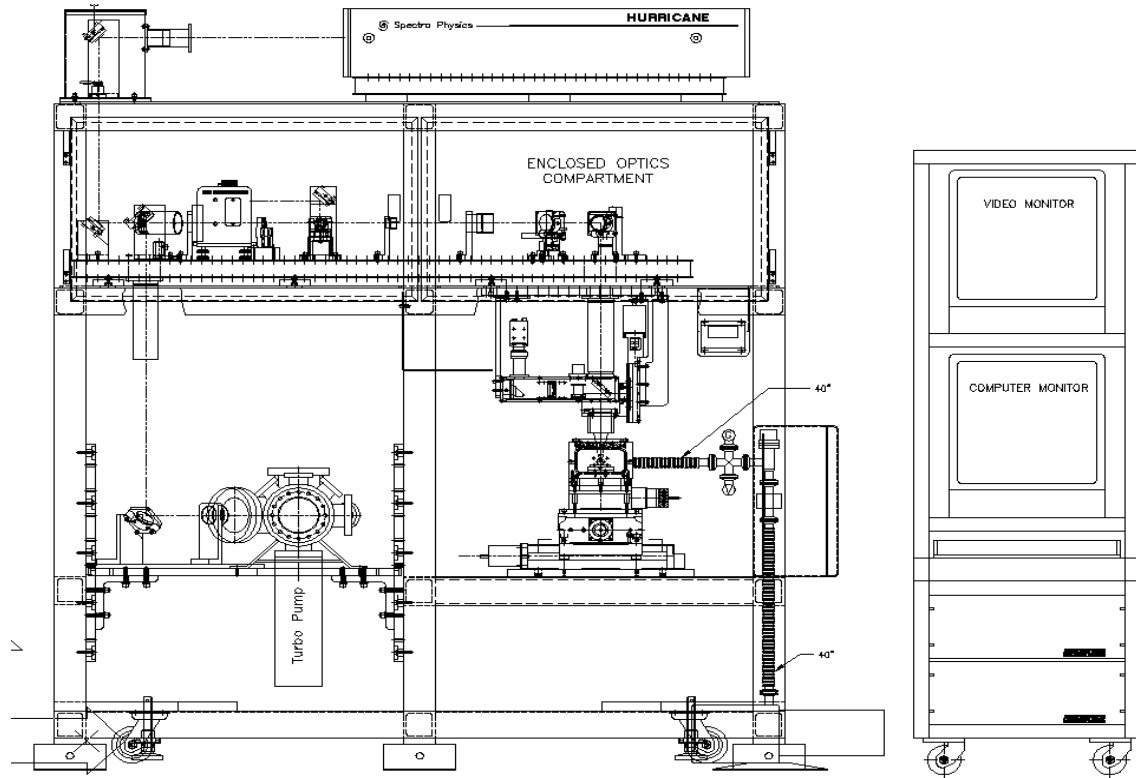


Figure 1 The femtosecond laser microfabrication system.

The femtosecond laser is positioned on the top shelf. This has been done to provide the shortest possible beam path while allowing for ease of access for servicing of the laser. There is also a provision for the beam from the seed laser to be extracted and delivered to the work area below for other experiments. Laser power supply and fiber-coupled pump laser are positioned beside the system and connected to it via umbilicals. On the top shelf provisions are made to allow addition of higher-harmonic modules to the laser. On exiting from laser, the beam first encounters safety shutter interlocked with the system covers and/or other safety sensors. Then the beam is directed via a two-mirror periscope towards the second shelf. This shelf supports the beam shaping optics. All optical elements are mounted on an optical breadboard for flexibility (See Fig.2). This shelf is enclosed, and this compartment is continuously purged with filtered air so that it remains clean and free of dust particles. A small HEPA filter and blower are integrated with the system for this purpose. After passing through an adjustable iris and a high-speed process shutter (Uniblitz VS14S2S1 by Vincent Associates, Rochester, NY) the laser beam arrives to two filter wheels, first of which provide for transmission of 1.0, 0.1, 0.03, 0.01 and 0.001 and second, of 0.1 to 0.9, in steps of 0.1. Beams reflected from filters are directed to absorbing light dumps. Following filters, a precision flip-in mirror is positioned which is used to direct the beam towards autocorrelator for monitoring and optimization of the pulse temporal profile, as described above. Further downstream the beam is expanded with a Galilean beam expander (negative eyepiece and positive collimating doublet). Three different expansion ratios (1x, 2x and 3x) can be achieved using two eyepiece assemblies and two collimating

assemblies in different combinations. Lens mounts are designed in such a way that only fine focussing of the final lens is needed after an expansion (and thus spot size) change. The laser beam is finally sent down by a folding mirror, through an opening in the middle shelf, into a focussing column attached to it (Fig.3). An achromatic objective (EFL = 75 mm, NA = 0.2) is used to focus the beam. The objective is infinity-corrected, diffraction limited and has a long working distance (~3.5"). Its aperture is 30 mm providing for minimal truncation of the (expanded) laser beam. With this lens and the different combination beam expanders, various focussed spot diameters (between 5 μm and 15 μm) can be achieved on target. The lens is mounted on a precision motorized vernier for focussing of the beam on the work piece. Entire beam focussing optics was developed and fabricated in cooperation with Special Optics (Wharton, NJ).

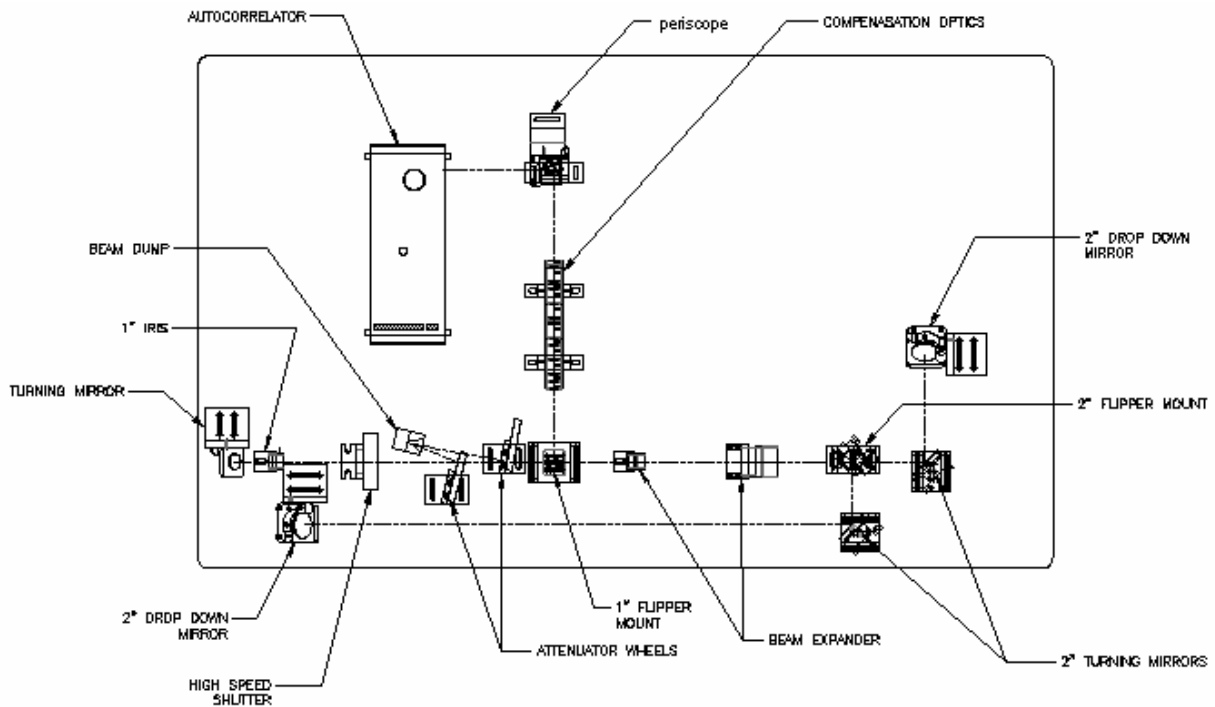


Fig.2 Optical set up of the middle shelf

The work piece is mounted inside a small vacuum chamber. The laser beam is focussed through an AR-coated transparent window. (This window's thickness and material properties were accounted for in the optical design both with respect to spot formation and the pulse's temporal characteristics). A vacuum pump is supplied to evacuate the chamber for laser processing. The vacuum chamber is mounted on an XY θ stack whose motion is controlled by the computer through CNC programming. Viewing of the sample and the alignment of the beam to it are performed through the same beam-focussing lens. A flat-plate dichroic beamsplitter is positioned between the folding-down mirror and the lens. It injects quasi-monochromatic visible illuminating light onto the work piece, which, after reflection from the work piece is re-imaged through the focussing objective and reflected by the same beamsplitter via a relay lens onto a CCD camera. A color filter in front of the camera protects the CCD sensor from laser radiation.

With the flip of a precision kinematic mirror mount, the laser beam after the beam expander can be redirected into a secondary focussing column. This column is pointing towards a large open workspace, which can be filled with customer supplied equipment. All electronics equipment controlling the system are installed in a 19-inch rack together with two monitors: one for the computer and another for the vision system.

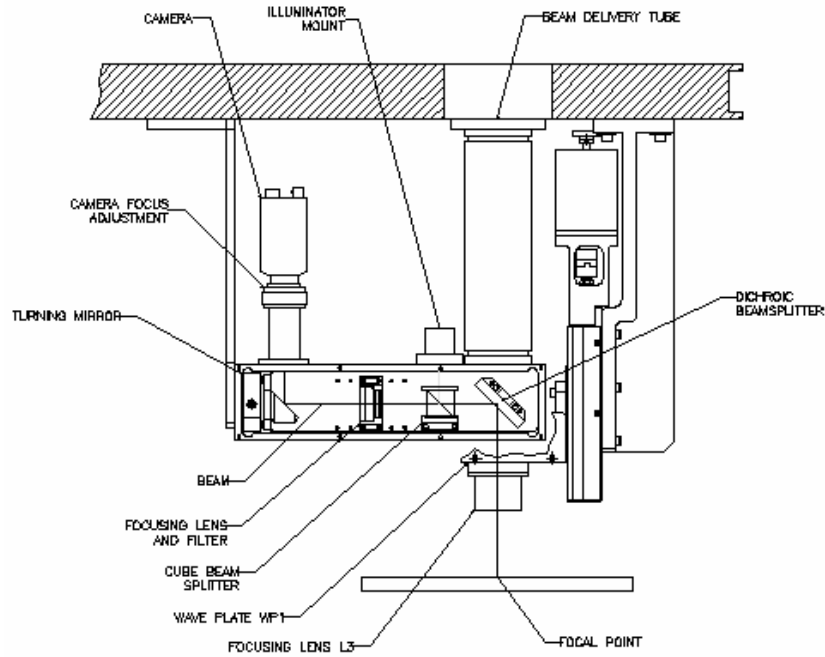


Figure 3 Focusing column of the femtosecond micromachining system

3. FEMTOSECOND PROCESSING OF STAINLESS STEEL

As the first example of femtosecond laser processing, we studied ablation regimes for drilling holes in 50 μm thick AISI 316 stainless steel (SS) in vacuum. First of all, we established the threshold of SS ablation. It is well known that for a laser beam with a Gaussian energy distribution, the diameter D of the ablated crater is related to the surface damage threshold fluence F_{th} , the incident laser fluence F_0 and the beam waist ω_0 by the following equation¹⁰⁻¹²:

$$D^2 = 2\omega_0^2 \ln(F_0/F_{\text{th}}) \quad (1)$$

The diameter D can be determined by scanning electron microscopy (SEM). This model yields a linear relationship in a semi-logarithmic plot of D^2 versus F_0 for $\omega_0 = 12 \mu\text{m}$ and $\omega_0 = 4 \mu\text{m}$, as shown in Fig. 4 (a).

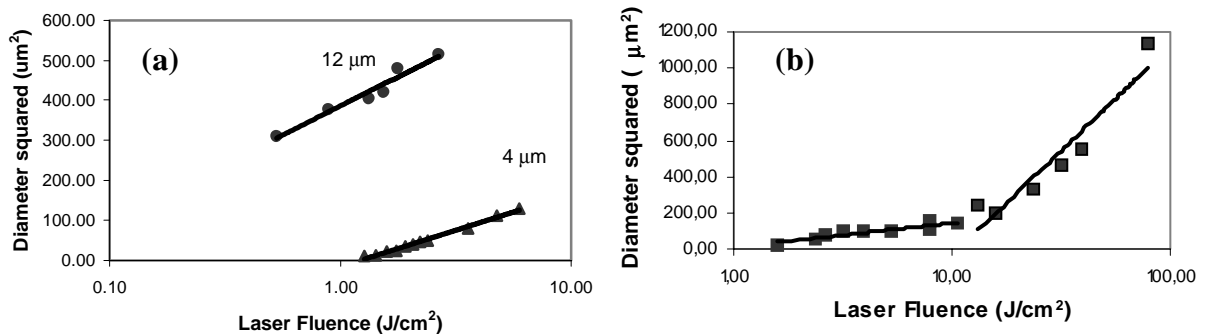


Fig. 4 Squared diameters D^2 of craters on the SS surface as a function of laser fluence F : (a) single laser shot, beam waists of 12 and 4 μm ; (b) 2000 shots at the same spot, the beam waist of 4 μm .

Using equation (1), we can determine the values for the threshold of 0.05 J/cm^2 for the waist $\omega_0 = 12 \text{ }\mu\text{m}$ and 1.2 J/cm^2 for $\omega_0 = 4 \text{ }\mu\text{m}$ under a single laser shot, whereas for 1000 shots the relevant values of F_{th} were 0.04 J/cm^2 and 0.45 J/cm^2 , respectively. These values are in good agreement with typical ablation thresholds from the literature^{13,14}. Notice that a lower threshold for 1000 shots is typical for the laser ablation and is explained by the morphological changes of the irradiated surface due to laser action, chemical reactions in the irradiation areas and incubation behaviour of pulses¹⁰⁻¹². The difference between thresholds for the two beam waists is probably related to different radiation energy deposition in the focal spot: as the beam waist get smaller, F_{th} has to be larger to compensate the net energy flux dissipated away from the beam center by the hot electrons diffusion. As follows from figure 4(b), at relatively high fluence the slope of the $D^2(F)$ line increases substantially, suggesting the existence of a faster ablation regime, as it has already been reported in some experiments on silver at lower fluences¹⁵. However, this hypothesis should be confirmed by the analysis of the total ablated volume per pulse, since higher increase rate for the crater diameter can be accompanied by the lower increase rate for the ablated depth per pulse, as it occurs during the ablation of silicon (see below). These studies are in progress.

Typical SEM images of holes drilled in SS are shown in Fig. 5. One can see that at relatively low laser fluences $I = 0.7 - 3 \text{ J/cm}^2$, the regime of a “gentle” ablation takes place. This regime is characterized by an exceptional quality of the ablated surface and a complete absence of “corona” due to thermal effects, which is typical for the nanosecond laser ablation of metals¹⁶. The ablation rate for this regime is relatively moderate and does not exceed 25 nm/pulse . This regime is especially efficient for the patterning of high-quality hole or line markers on surfaces. However, the ablation rate in this regime is not sufficient to drill rapidly deep or through holes, which is important in some industrial applications. On the other hand, the ablation rate at larger fluences $I > 5 \text{ J/cm}^2$ increases to $30-100 \text{ nm/pulse}$, which is high enough to effectively produce, for example, through holes or deep channels for industrial applications. The profile of typical through hole in a $50\text{-}\mu\text{m}$ thick SS foil, drilled at $F = 15 \text{ J/cm}^2$ is shown in Fig. 6. It can be clearly seen that the walls of the hole are free from debris and heat-related effects. However, we found that drilling at very high fluences $F > 15 \text{ J/cm}^2$ can be accompanied by parasitic ablations around the focal spot, which are not significant at moderate fluences $10 - 15 \text{ J/cm}^2$ as seen in Fig. 5. The parasitic ablation effects are probably related to the residual radiation intensity at the tail of a Gaussian distribution or to the generation of Rowland ghost because of the non-ideality of the diffraction gratings inside the laser resonator¹⁷. The presence of the parasitic effects requires the application of additional methods of the beam cleaning to assure high quality of the laser processing.

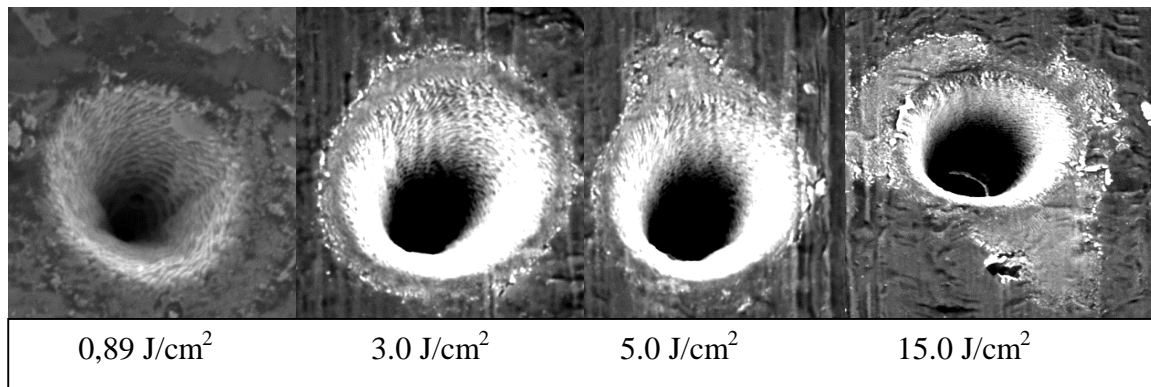


Fig. 5 Scanning electron microscope (SEM) images of holes in a $50 \text{ }\mu\text{m}$ thick SS foil performed under different laser fluences by 2000 laser pulses in vacuum. The beam waist was $12 \text{ }\mu\text{m}$.

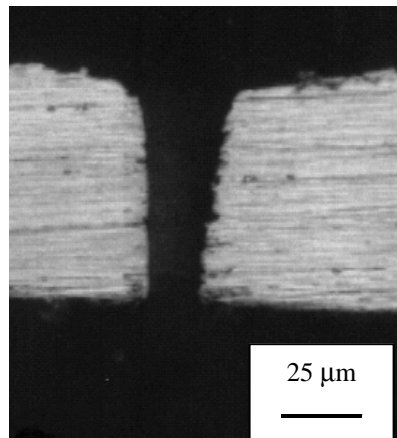


Fig. 6 SEM image of the cross section of a hole drilled in a 50 μm thick SS foil at the fluence of 15 J/cm² and beam waist of 12 μm.

4. FEMTOSECOND PROCESSING OF SILICON

4.1 Hole formation in silicon

As another example of femtosecond laser processing, we studied the ablation of silicon. Figure 7 shows typical atomic force microscope (AFM) images of craters formed on a silicon (111) target. One can see that for all fluences except of very low ones ($F < 0.4 \text{ J/cm}^2$) the holes had a symmetric profile and the walls of holes were free of debris. Certain deviation from a symmetric hole profile at low fluences was apparently related to a non-uniform surface absorption under near threshold conditions. The diameter of craters and their depth increased as the laser fluence increased, which is consistent with previous studies. It should be noted that a layer of redeposited material can be clearly seen around all holes, while for very high fluences $F > 20 \text{ J/cm}^2$ the layer transformed to fountain-like structure of deposited material. Similar results were obtained for the processing of Si (100).

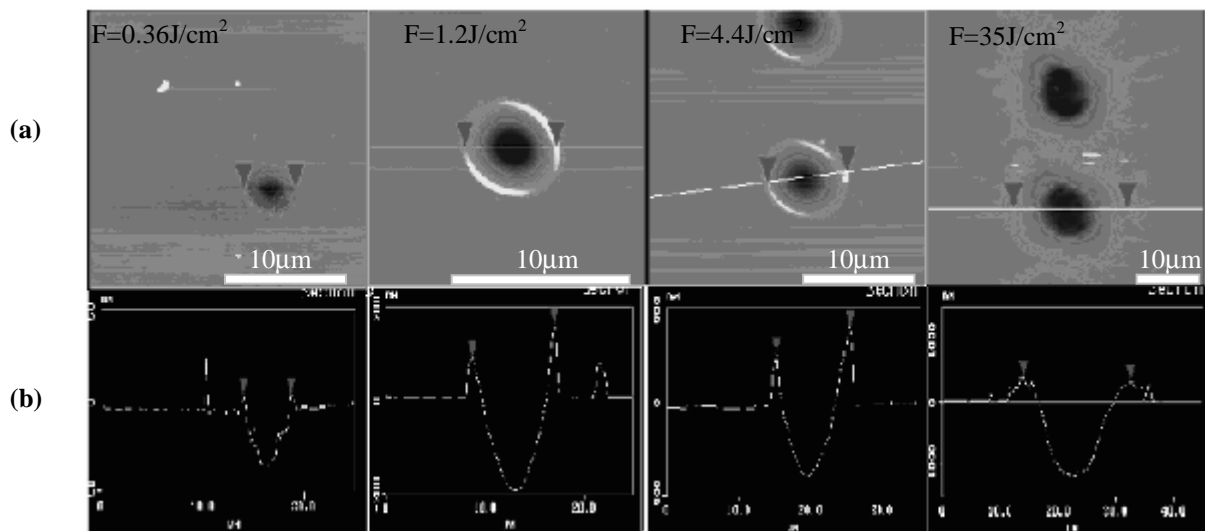


Fig. 7 Typical AFM images of ablated Si (111) surface (a) and the cross-section profile along the indicated white line (b) for various laser fluences.

The data on the diameter squared D^2 of the holes as a function of the laser fluence of a single shot (for low fluences below 5 J/cm^2) are shown in Fig. 8 for silicon (111) and (100) surfaces. Using equation (1), we can determine the ablation threshold fluences F_{th} , which were $(0.21 \pm 0.01) \text{ J/cm}^2$ for $\omega_0 = 4\mu\text{m}$ and $(0.11 \pm 0.01) \text{ J/cm}^2$ for $\omega_0 = 12\mu\text{m}$. This last value is in good agreement with threshold values, which are usually cited in the literature for 100 fs pulses^{18,19}. It should be mentioned that the ablation rates and thresholds were essentially independent of the crystal orientation

As follows from Fig. 8 (c), the slope of the line $D^2(F)$ increases for $F > 5 \text{ J/cm}^2$. Note that similar phenomenon was observed with SS, as shown in Fig. 4(b). However, the examination of the depth of craters shows that the ablation at fluences higher than 5 J/cm^2 is accompanied by the loss of the depth rate, as illustrated in Fig. 9 (a). As a consequence, the increase rate for the resulting ablated volume remains the same, as one can see from Fig. 9 (b). Finally, Fig. 9(c) illustrates that the strongest variation of the Depth/Diameter ratio occurs in the laser fluence range of 1 to 10 J/cm^2 . Considering optimal regime for silicon processing, a fluence of about 5 J/cm^2 seems to be preferable to produce high quality craters at a relatively high ablation rate.

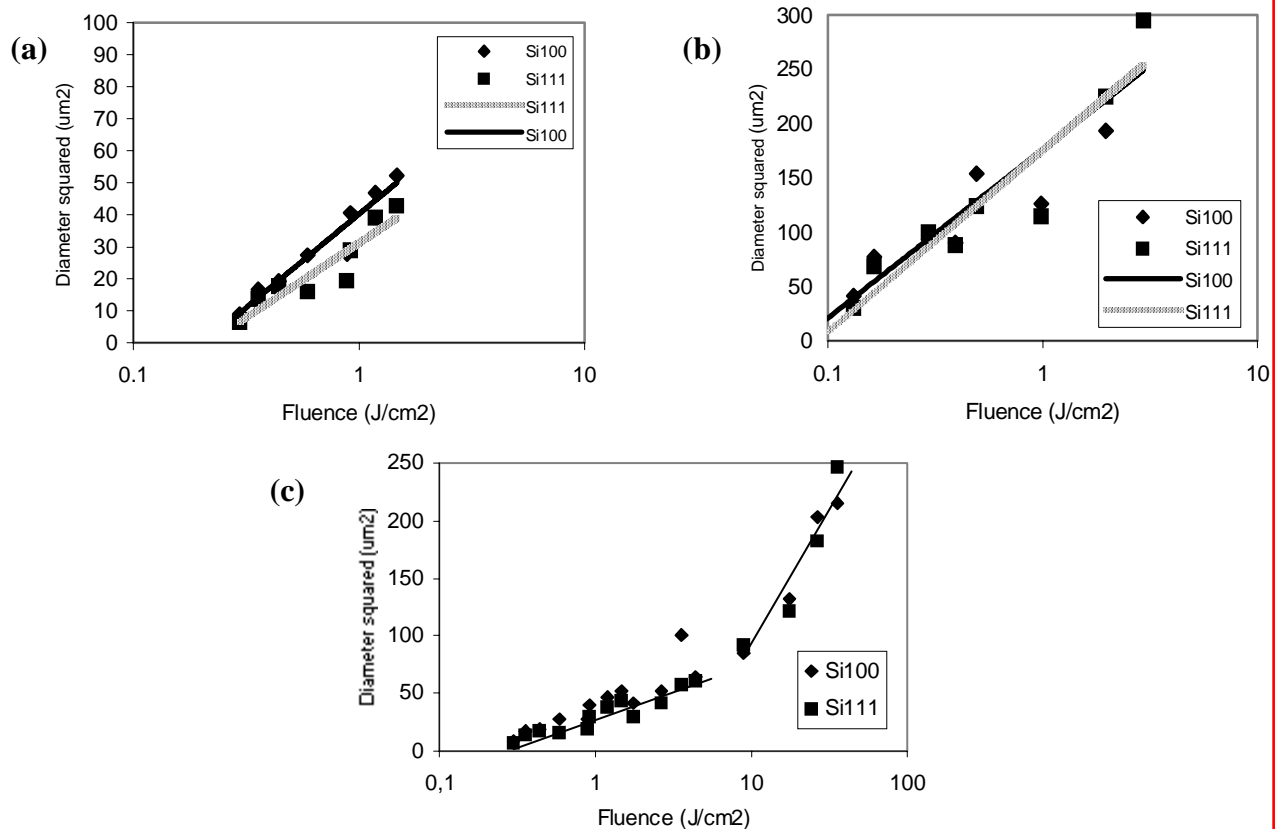


Fig. 8 Squared diameter of craters on Si (111) and Si (100) as a function of incident laser fluence for $\omega_0 = 4\mu\text{m}$ (a) $\omega_0 = 12\mu\text{m}$ (b), $\omega_0 = 4\mu\text{m}$, high fluences (c). All dependencies are given for a single laser shot

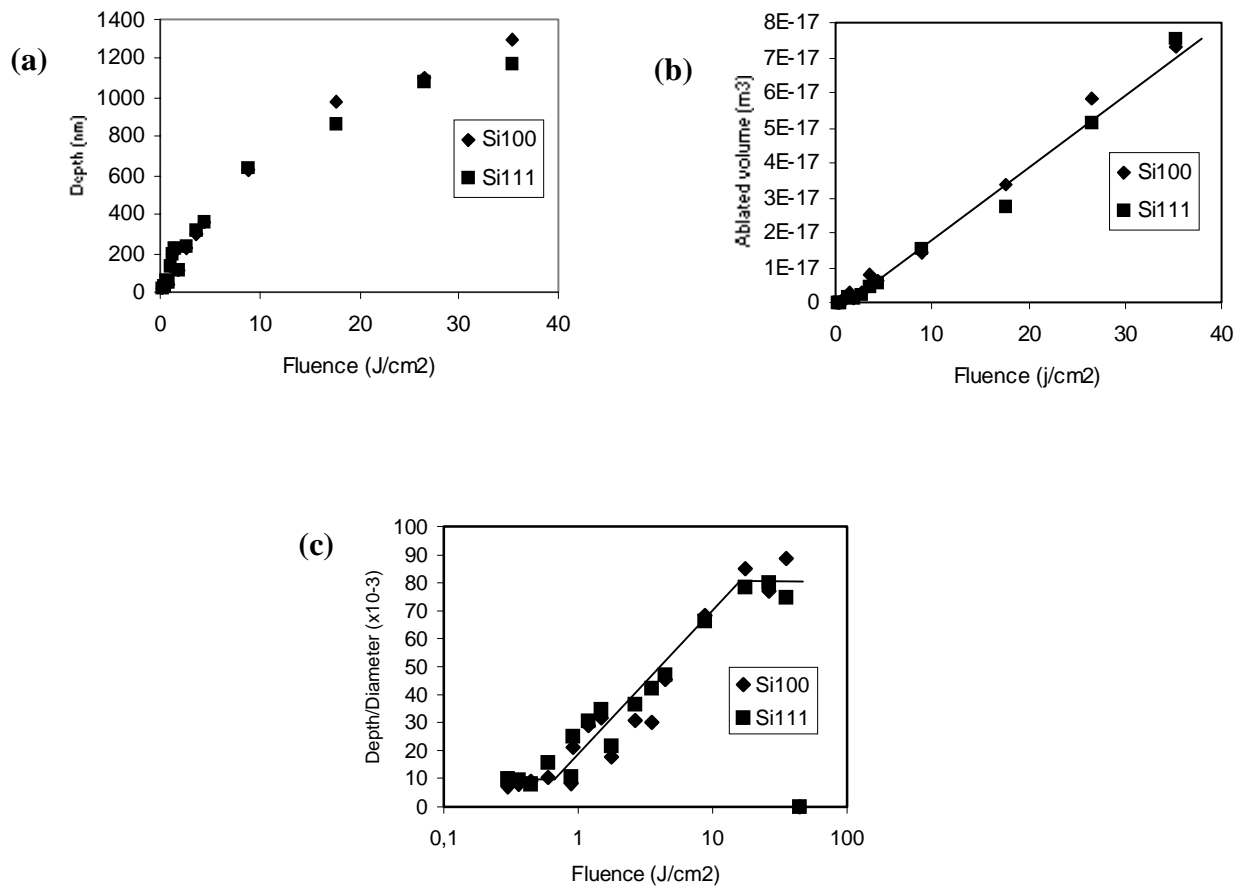


Fig. 9 Ablation of Si (111): Depth of ablated crater (a), total ablated volume (b) and the depth-to-diameter ratio as a function of the laser fluence. The dependencies are given for a single laser shot and the waist diameter of 4 μm .

4.2 Cutting of thin silicon wafers

By now it is actively discussed that the use of very thin silicon wafers (50 μm thick and less) can help to increase the circuit density of modern microelectronics²⁰. Since these thin wafers are very fragile, conventional mechanical cutting techniques, such as the one using a diamond saw, must be avoided. Femtosecond laser seems to be very promising to perform this task due to the absence of the heat-affected zone and limited induced mechanical stress. We examined the efficiency of cutting of 50 μm thick Si wafers by our micromachining system. The main attention was given on the optimization of laser ablation parameters such as the fluence, number of pulses and cutting speed. To accomplish this task, we used a beam with a circular polarization to obtain a uniform cutting²¹. Figure 10 shows both the front and rear side of silicon cuts performed at different laser fluences in vacuum. Each cut consisted of 150 passages to be able to compare low and high fluences; at a scanning speed of 300 $\mu\text{m/s}$, this gives a net cutting speed of 2 $\mu\text{m/s}$. Note that the walls of the cut had an angle of about 80° with the wafer surface, which was almost independent of the laser fluences.

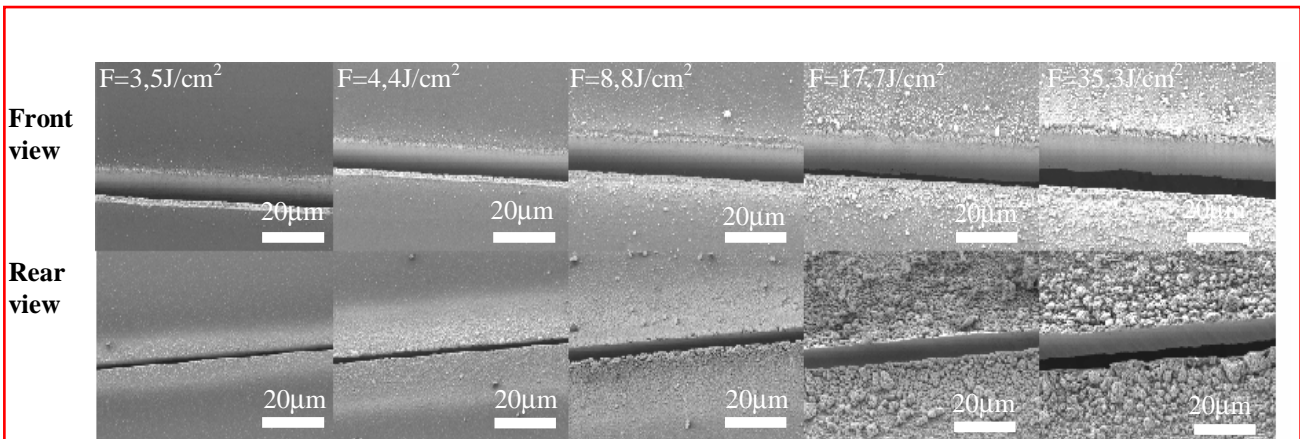


Fig. 10 SEM images of cut edges on a 50 μm thick Si(111) wafer from its front and rear sides performed at different laser fluences, with a spot size of 4 μm , a scanning speed of 300 $\mu\text{m/s}$ and 150 passages.

Figure 11 illustrates the effect of the number of passes at a constant fluence of 4.4 J/cm², which was selected to avoid the production of large particles. One can see that the best quality of the wafer cut is achieved after 40 passes, while a further increase of the number of passes leads to an increase of the cut width from 3 to 5 μm without any affect on the cut quality. In these conditions, the minimal net cutting speed was about 8 $\mu\text{m/s}$. Note that the net cutting speed can be significantly increased if one splits the beam and performs several cuts simultaneously. With our system this is possible since we used only about 1% of the maximum laser fluence.

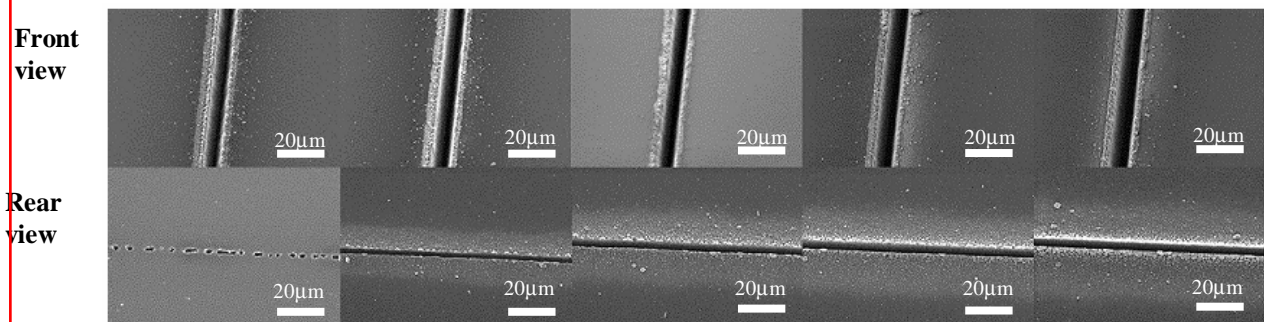


Fig. 11 SEM images of cut edges on a 50 μm thick Si(111) wafer from its front and rear sides after 20, 40, 60, 80 and 100 passages. The focal spot size and the scanning speed were 4 μm and 300 $\mu\text{m/s}$, respectively.

5. CONCLUSION

A new automated femtosecond laser micromachining system was designed for micromachining of industrially important materials. First tests of the systems on the drilling of fine holes and cutting of stainless steel and silicon are presented. Two regimes were noticed in the ablation process for the two materials investigated. In the “gentle” ablation regime, slow ablation rates (25 nm/pulse for SS and silicon) are obtained with a very limited HAZ. Above a certain fluence (5-10 J/cm²), a “fast” ablation regime leads to a substantial increase of the hole diameter for both stainless steel and silicon samples. In the case of silicon, it also leads to the appearance of large particles. As industrial micromachining examples, we successfully made fine through holes in 50 μm thick SS and cut 50 μm thick silicon at a speed of 8 $\mu\text{m/s}$, both presenting essentially no HAZ. The system is well suited for a large number of applications in microelectronic and microelectromechanical systems.

REFERENCES

1. J. Bonse, S. Baudach, J. Krüger and W. Kautek. "Femtosecond laser micromachining of technical materials", *Proc. SPIE*. **4065**, pp. 161-172, 2000.
2. S. Küper and M. Stuke, "Femtosecond uv excimer laser ablation", *Appl. Phys. B* **44**, pp. 199-204, 1987.
3. P. Schwab, J. Heitz, S. Proyer, and D. Bäuerle. "Femtosecond-excimer-laser patterning of Yba₂Cu₃O₇ films", *Appl. Phys. A* **53**, pp. 282-283, 1991.
4. S. Preuss, E. Matthias, and M. Stuke. "Sub-picosecond UV-laser ablation of Ni films", *Appl. Phys. A* **59**, pp. 79-82, 1994.
5. W. Kautek and J. Krüger. "Femtosecond-pulse laser ablation of metallic, semiconducting, ceramic, and biological materials", *Proc. SPIE* **2207**, pp. 600-611, 1994.
6. J. Ihlemann, A. Scholl, H. Schmidt, and B. Wolff-Rottke. "Nanosecond and femtosecond excimer laser ablation of oxide ceramics", *Appl. Phys. A* **60**, pp. 411-417, 1995.
7. J. Ihlemann, B. Wolff, and P. Simon. "Nanosecond and femtosecond excimer laser ablation of fused silica", *Appl. Phys. A* **54**, pp. 363-368, 1992.
8. J. Krüger and W. Kautek, "Femtosecond pulses visible laser processing of fibre composite materials", *Appl. Surf. Sci.* **106**, pp. 383-389, 1996.
9. D. Stern, R.W. Schoenlein, C.A. Puliafito, E.T. Dobi, R. Birngruber and J.G. Fujimoto. "Corneal ablation by nanosecond, picosecond, and femtosecond lasers at 532 and 625nm", *Arch. Ophthalmol.* **107**, pp. 587-592, 1989.
10. N. Rizvi, D. Kakis, C. Gower. "Micromachining of industrial materials with ultrafast lasers". In ICALEO 2001
11. C. Momma, S. Nolte, B. Chichkov "Precise laser ablation with ultrashort pulses", *Appl. Surf. Sci.*, **109**, pp. 15-19, 1997.
12. P. Pronko, S. Dutta, J. Squier "Machining of sub-micron holes using a femtosecond laser at 800nm.", *Optics Commun.*, **114**, pp. 106-110, 1995.
13. S.M. Klimentov, T.V. Kononenko, P.A. Pivovarov, S.V. Garnov, V.I. Konov, A.M. Prokhorov, D. Breitling and F. Dausinger, "The role of plasma in ablation of materials by ultrashort laser pulses", *Quantum Electronics* **31** pp.378-382, 2001
14. P.S. Banks, M.D. Feit, A.M. Rubenchik, B.C. Stuart and M.D. Perry. "Material effects in ultra-short pulse laser drilling of metals", *Appl. Phys. A* **69**, pp. S377-S380, 1999.
15. K. Furusawa, K. Takahashi, H. Kumagai, K. Midorikawa and M. Obara. "Ablation characteristics of Au, Ag, and Cu metals using a femtosecond Ti:sapphire laser", *Appl. Phys. A* **69** S359-S, 1999.
16. B. Chichkov, C. Momma, S. Nolte, F. von Alvensleben, A. Tunnermann "Femtosecond, picosecond and nanosecond laser ablation of solids", *Appl. Phys. A*, **63**, pp. 109-115, 1996.
17. B. K. A. Ngoi, K. Venkatakrisnan, B. Tan and N. R. Sivakumar. "The effect of Rowland ghosts on sub-micron-machining using femtosecond pulsed laser", *Optic express*, **8**, pp. 492-496, 2001.
18. M. C. Downer, C. V. Shank, "Ultrafast heating of silicon on sapphire by femtosecond optical pulses", *Phys. Rev. Lett.*, **56**, pp. 761-764, 1986.
19. C. V. Shank, R. Yen, C. Hirlimann, "Time resolved reflectivity measurements of femtosecond pulse induced phase transition in silicon", *Phys. Rev. Lett.*, **50**, pp. 454-457, 1983.
20. J. Young, A. Malshe, W. Brown, "Thermal modeling and mechanical analysis of very thin silicon chips for conformal electronic systems packaging". HD International Conference and Exposition on High Density Interconnects and System Packaging. Santa Clara, CA, April 2001.
21. Tonshoff, H. K; Ostendorf, A; and Wnager, T. "Structuring silicon with femtosecond lasers". In : *Proc. SPIE*, **4274**, pp. 88-97, 2001.